

Supplementary Figures

Supplementary Fig. 1. Flow cytometric analyses of innate lymphoid cell subsets in B16-OVA and SM1WT melanoma tumor-bearing mice.

a-f, Flow cytometric analyses of immune cell subsets from B16-OVA (**a-c**) and SM1WT1 (**d-f**) tumor-bearing C57BL/6J mice. **a** and **d**, Representative gating strategy used to define ILC subsets. **b,c,e**, and **f**, Enumeration (left panels) and frequency (right panels) of tumor-infiltrating ILCs (**b** and **e**) and NK cells, ILC1, ILC2 and ILC3 from control and tumor-draining lymph nodes (**c** and **f**) isolated from B16-OVA (tumor, $n=17$; lymph nodes, $n=18$) (**b** and **c**) and SM1WT1 (Tumor, $n=12$; Lymph nodes, $n=18$) (**e** and **f**) tumor-bearing mice 8 and 6 days after tumor inoculation, respectively. Data are pooled from two independent experiments with 6-12 mice/experiment/cell line. Each circle represents one mouse and data show the mean \pm s.e.m. **c** and **f**, Statistical analyses were performed using paired Student's t tests. p values are indicated.

Supplementary Fig. 2. Mass cytometry gating strategy used to identify ILC subsets in human metastatic melanoma tumors.

a and **b**, Mass cytometric analyses of NK cells, ILC1, ILC2 and ILC3 from prospectively collected human metastatic melanoma lesions. **a**, Gating strategy used to identify NK cells, ILC1, ILC2 and ILC3. NK cells were identified as live CD45⁺CD3⁻CD19⁻CD56⁺Eomes⁺; ILC1 were identified as live CD45⁺lin⁻(CD3⁻CD19⁻CD11c⁻CD11b⁻CD14⁻CD15⁻CD33⁻CD68⁻CD123⁻CD56⁻CD4⁻CD8a⁻TCRgd⁻TCRVa7.2⁻TCRb⁻)HLA-ABC⁺EOMES⁺T-BET⁺; ILC2 were identified as live CD45⁺Lin⁻HLA-ABC⁺EOMES⁻T-BET⁻CD161⁺RORgt⁺; and ILC3 were identified as live CD45⁺Lin⁻HLA-ABC⁺EOMES⁻T-BET⁻CD161⁺RORgt⁺. **b**, Mass cytometry contour plots showing CD161 expression in CD161-non expressing B cells and CD161-expressing T cells. For two patient samples CD11c in the lineage panel was replaced by HLA-DR. For five other patients, CD3 in the lineage panel was not used.

Supplementary Fig. 3. *NCR^{iCre/+}Mcl1 Δ/Δ* mice are deficient in tumor-infiltrating NKp46-expressing cells.

a-c. Flow cytometric analyses of splenic and tumor infiltrating immune cells from C57BL/6J, *NCR^{iCre}Mcl1^{+/+}* and *NCR^{iCre}Mcl1 Δ/Δ* mice. **a** and **c**, t-Distributed stochastic neighbour embedding (t-SNE) plots were generated from FlowJo using standard parameters. Live CD45⁺ cells from each sample were downscaled to 5×10^3 events, concatenated and t-SNE plots were then generated using CD3 ϵ , TCR β , CD19, NK1.1, NKp46, CD49b, CD49a and KLRG1 surface expression. **b**, Flow cytometric contour plots showing NK1.1⁺ and NKp46⁺ splenic and tumor-infiltrating NK cells and ILC1 in C57BL/6J, *NCR^{iCre}Mcl1^{+/+}* and *NCR^{iCre}Mcl1 Δ/Δ* mice. Cells were gated on live CD45⁺CD3 ϵ ⁺TCR β ⁻. Data show one of 2 independent experiments with similar results.

Supplementary Fig. 4. Purification of bone marrow-derived progenitors.

Bone marrow-derived progenitors were first enriched based on IL-7R expression using magnetic separation and then cell sorted using a BD FACSAria cell sorter. Flow cytometric contour plots showing the gating strategy used to purify common lymphoid progenitor [CLP: lin⁻(CD3 ϵ ⁻B220⁻CD11b⁻TER119⁻NKp46⁻F4/80⁻CD19⁻TCR β ⁻NK1.1⁻)CD127⁺Flt3⁺a4b7⁻CD117⁺], a-lymphoid progenitors (aLP) [lin⁻CD127⁺Flt3⁺a4b7⁺CD117⁺CD25⁻] and ILC2 progenitors (ILC2p) [lin⁻CD127⁺Flt3⁺a4b7⁺CD117⁺CD25⁺Sca-1⁺]. Analysis of purity was performed after cell sorting. Plots are representative of 6 similar experiments.

Supplementary Fig. 5. Intestinal immune cell subsets in C57BL/6J, *Rag1*^{-/-} and *Rag2*^{-/-}*Il2rg*^{-/-} mice reconstituted with bone marrow-derived progenitors isolated from CD45.1 mice.

Analyses of intestinal immune cell populations in C57BL/6J, *Rag1*^{-/-}, *Rag2*^{-/-}*Il2rg*^{-/-} and *Rag2*^{-/-}*Il2rg*^{-/-} mice reconstituted with bone marrow-derived ILC2p, aLP or CLP. **a**, Representative flow cytometric contour plots of immune cells isolated from the intestinal lamina propria of C57BL/6J mice showing the gating strategy used to identify different subsets. Plots are gated on live CD45.1⁺CD45.2⁺ cells. **b**, Frequency of T cells, B cells, myeloid cells, NCR⁺ and NCR⁻ILC3, ILC2, and NK cells/ILC1 (NKp46⁺RORγt⁺ cells) identified as described in **a**. Data show one representative experiment (C57BL/6J, *n*=6 mice; *Rag1*^{-/-}, *n*=4 mice; *Rag2*^{-/-}*Il2rg*^{-/-}, *n*=2 mice; *Rag2*^{-/-}*Il2rg*^{-/-}+ILC2p, *n*=3 mice; *Rag2*^{-/-}*Il2rg*^{-/-}+aLP, *n*=2 mice; *Rag2*^{-/-}*Il2rg*^{-/-}+CLP, *n*=2 mice) of 6 in which bone marrow-derived progenitors were transferred into recipient mice. Each dot represents one mouse and data show mean ± s.e.m. **c**, Representative flow cytometric contour plots showing the fraction of CD45.1⁺ and CD45.2⁺ proportion of each subset within each immune cell population from the different strains of mice. Blank plots represent immune cell subsets that are absent in the indicated mice as shown in **b**.

Supplementary Fig. 6. Key transcriptional features of tumor-infiltrating ILC2 identified using scRNA sequencing.

a-d, Single cell RNA sequencing analysis of 2,261 tumor infiltrating leukocytes purified by flow cytometric sorted from two BRAF^{CA};PTEN^{loxP};Tyr::CreER^{T2} tumors collected 48 days after treatment with tamoxifen. **a,c** t-SNE plots showing log₂ normalized expression of T cells and ILC surface markers *Cd3d*, *CD3g*, *CD3e*, *Cd247*, *Cd8a*, *Cd4*, *Ncr1* and transcription factors/transcriptional regulators *Foxp3*, *Rorc*, *Id2*, *Gata3* and *Rora*. **b,d** Representative differentially expressed gene (*y*-axis) expression for different T cell and ILC subsets (*x*-axis) as identified in Fig 3a. Dot size represents the fraction of cells within the population that express each gene. Colors indicate the z-scaled expression of genes in cells within each subset.

Supplementary Fig. 7. ILC2 express high levels of GM-CSF in B16-OVA and SM1WT1 tumors.

a and **f**, Representative flow cytometric gating strategy used to identify GM-CSF-expressing ILC2 in B16-OVA (**a**) and SM1WT1 (**f**) melanoma tumors 8 and 6 days after tumor inoculation, respectively. GM-CSF expression in other immune and non-immune cell subsets is also depicted. **b** and **f**, Frequency of GM-CSF-producing cells in B16-OVA (**b**) and SM1WT1 (**f**) melanoma tumors. **c** and **g**, Representative flow cytometric gating strategy used to identify polyfunctional (IL-5⁺IL-13⁺GM-CSF⁺) ILC2. **d** and **h**, Frequency of IL-5⁺, IL-13⁺ and GM-CSF⁺ILC2 and polyfunctional ILC2 (IL-5⁺IL-13⁺GM-CSF⁺) in lungs and B16-OVA (lungs, *n*=18, tumor, *n*=16) (**b**) or SM1WT1 (lungs, *n*=12, tumor, *n*=11) (**f**) tumors. **a-c**, Single cell suspensions of digested lung and tumor cells were stimulated with 50 ng/ml PMA, 500 ng/ml ionomycin in the presence of GolgiStopTM for 4h before intracellular staining for IL-5, IL-13 and GM-CSF. **b**, **d**, **f**, and **h**, Each circle represents one mouse and data show mean ± s.e.m. Data are pooled from two independent experiments with 5-12 mice/experiment. **d** and **h**, Statistical analyses were performed using paired Student's *t* tests. *p* values are indicated.

Supplementary Fig. 8. Eosinophils are absent from *PHIL* mice.

a, Representative flow-cytometric contour plots and frequency of circulating eosinophils from C57BL6 ($n=4$) and eosinophil-deficient *PHIL* ($n=7$) mice. **b-c**, Representative flow cytometric contour plots and enumeration of myeloid subsets in the spleen (**b**) and tumors (**c**) of C57BL/6J ($n=4-5$) and *PHIL* ($n=6$) mice at day 7 after Ret tumor inoculation. **d**, Enumeration of leukocytes and indicated lymphoid immune cell subsets in the spleen and tumors of C57BL6J ($n=5$) and *PHIL* ($n=6$) mice at day 7 after Ret tumor inoculation. Data show mean \pm s.e.m and are pooled from two experiments (**a**) or represents one experiment (**b-d**) with 2-6 mice/genotype/experiment. Statistical analyses were performed using unpaired Student's *t* tests. *p* values are indicated.

Supplementary Fig. 9. ILC2-derived GM-CSF enhances eosinophil cytotoxic functions.

In vitro analysis of the role of GM-CSF produced by intestinal ILC2 on the expression of eosinophil cytotoxic genes. **a**, Experimental design. Intestinal ILC2 were flow-cytometric sorted from C57BL/6J and *Csf2*^{-/-} mice and cultured for 2 days with 40 ng/ml of rIL-7 and IL-33 in complete media (8.5×10^3 cells/ well). ILC2 were identified as CD45⁺CD3⁻CD19⁻TCR β ⁻CD11b⁻NK1.1⁻c-kit⁺CD90.2⁺CD127⁺KLRG1⁺ cells. After two days of culture, ILC2-conditioned media was collected and added to fresh complete media (ratio 1:1) to culture purified splenic eosinophils. ILC2 were harvested and (**b,c**) GM-CSF and IL-5 expression was analyzed using flow cytometry. **b**, Representative flow cytometric histograms (left panel) and quantification (middle and right panels) of GM-CSF expression in C57BL/6J and *Csf2*^{-/-} ILC2. **c**, Frequency (left panel) and geometric mean fluorescence intensity (gMFI, right panel) of IL-5-expressing C57BL/6J and *Csf2*^{-/-} ILC2. **b,c**, Data are pooled from 2 independent experiments with 1-4 biological or technical replicates/genotype/experiment. **b,c**, Statistical differences were assessed using unpaired Student's *t* tests and exact *p*-values are indicated.

Supplementary Fig. 10. Tumor-infiltrating T cells and ILC2 express high levels of PD-1 in B16-OVA and SM1WT1 tumors.

Flow cytometric analyses of PD-1 expression on tumor-infiltrating T cells and ILC2 isolated from B16-OVA and SM1WT1-tumor bearing mice 8 (**a**) or 6 days (**b**) after tumor inoculation, respectively. (**a, b**) Representative flow cytometric contour plots (left panels) and frequency (right panels) of PD-1 expression on tumor-infiltrating T cells and ILC2 isolated from B16-OVA (**a**) and SM1WT1 (**b**) tumor-bearing mice. Data are pooled from 2 independent experiments with 6-11 mice/experiment (B16-OVA, $n=17$ mice; SM1WT1, $n=12$ mice). (**a, b**) Each circle represents one mouse and data show the mean \pm s.e.m.

Supplementary Fig 11. Model linking the ILC2-Eosinophil axis to anti-tumor immunity in melanoma.

IL-5- and GM-CSF-derived ILC2 expressions induce eosinophil tumor recruitment, survival and function promoting anti-tumor responses. The combination of IL-33-driven ILC2 stimulation with anti-PD-1 antibody increases inflammatory KLRG1⁺ILC2 tumor infiltration and function, enhancing the recruitment of eosinophil into tumors further improving anti-tumor immunity.

Supplementary Tables

Supplementary Table 1. Patient characteristics.

Primary human melanoma tumors			
		<i>n</i> (%)	
Gender	Female	8 (40%)	
	Male	12 (60%)	
Age at diagnosis	<60	14 (70%)	
	≥60	6 (30%)	
Melanoma subtype	Superficial Spreading	12 (60%)	
	Nodular	4 (20%)	
	Lentigo maligna	1 (5%)	
	Desmoplastic	1 (5%)	
	Other	2 (10%)	
Molecular subtype	Wildtype	11 (55%)	
	NRAS	4 (20%)	
	BRAF	5 (25%)	
Stage at sampling	IA	4 (20%)	
	IB	14 (70%)	
	IIA	2 (10%)	
Recurrence	No	12 (60%)	
	Yes	8 (40%)	
Metastatic human melanoma tumors			
Gender	Female	5 (50%)	
	Male	5 (50%)	
Melanoma subtype	Unknown	2 (20%)	
	Mucosal	1 (10%)	
	Cutaneous	7 (70%)	
Molecular subtype	Wildtype	1 (10%)	
	NRAS mutated*	5 (50%)	
	BRAF mutated [#]	4 (40%)	
Stage at sampling	III	6 (60%)	
	IV	4 (40%)	
Tumor localization	Metastatic lymph node	8 (80%)	
	Subcutaneous metastasis	2 (20%)	
Previous treatment	No	5 (50%)	
	Yes	Immunotherapy	4 (40%)
		Targeted therapy	1 (10%)

n (%): Number of patients at risk (and proportion). *Mutations include NRASQ61R, NRASQ61L or NRASQ61K. [#]Mutations include BRAFV600E or BRAFV600K.

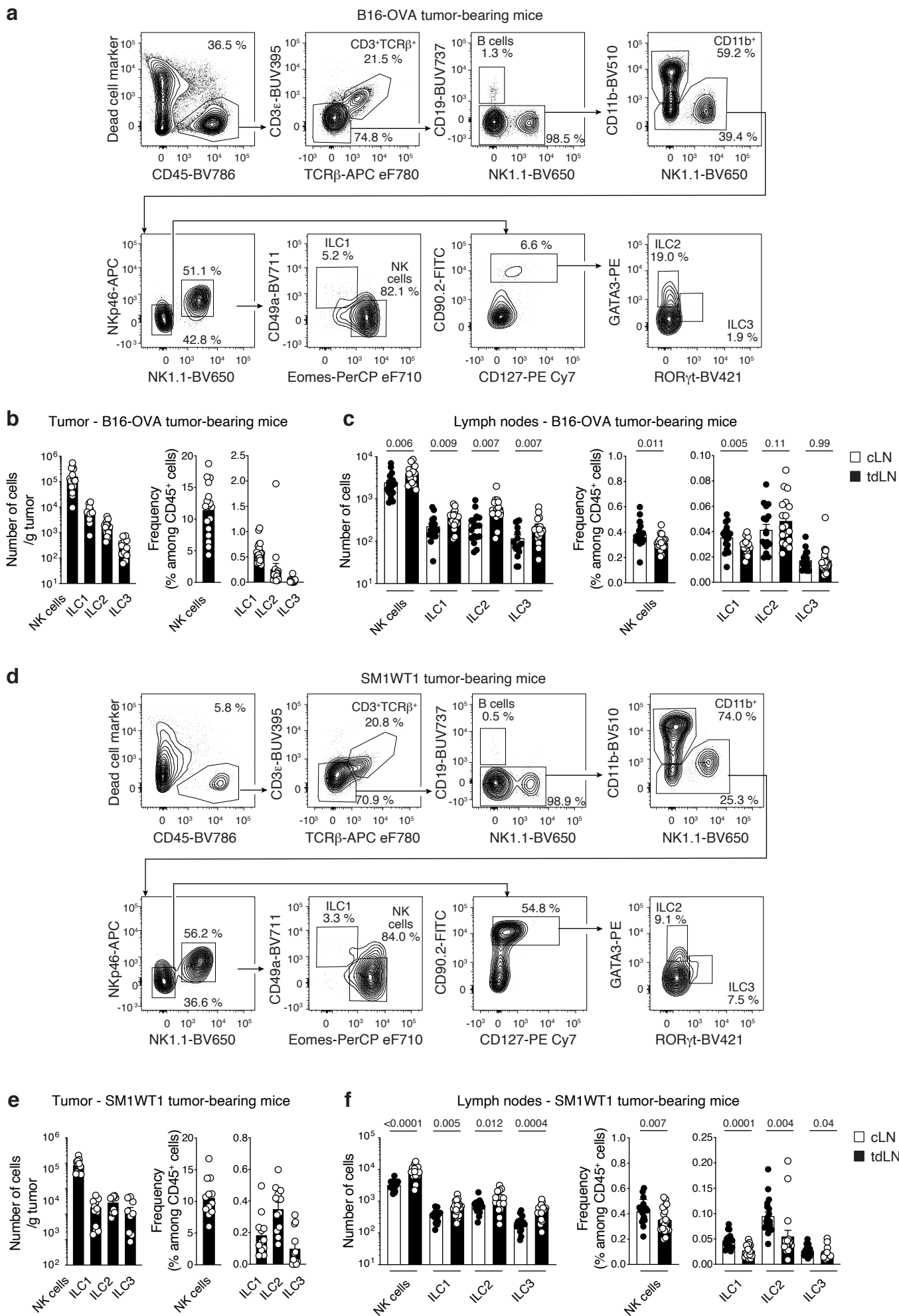
Supplementary Table 2. Cross-sectional tumor size statistical analyses of C57BL/6J, *Rag1*^{-/-} mice and *Rag2*^{-/-}*γc*^{-/-} mice, or *Rag2*^{-/-}*γc*^{-/-} mice reconstituted with CLP, αLP or ILC2p bone marrow-derived progenitors.

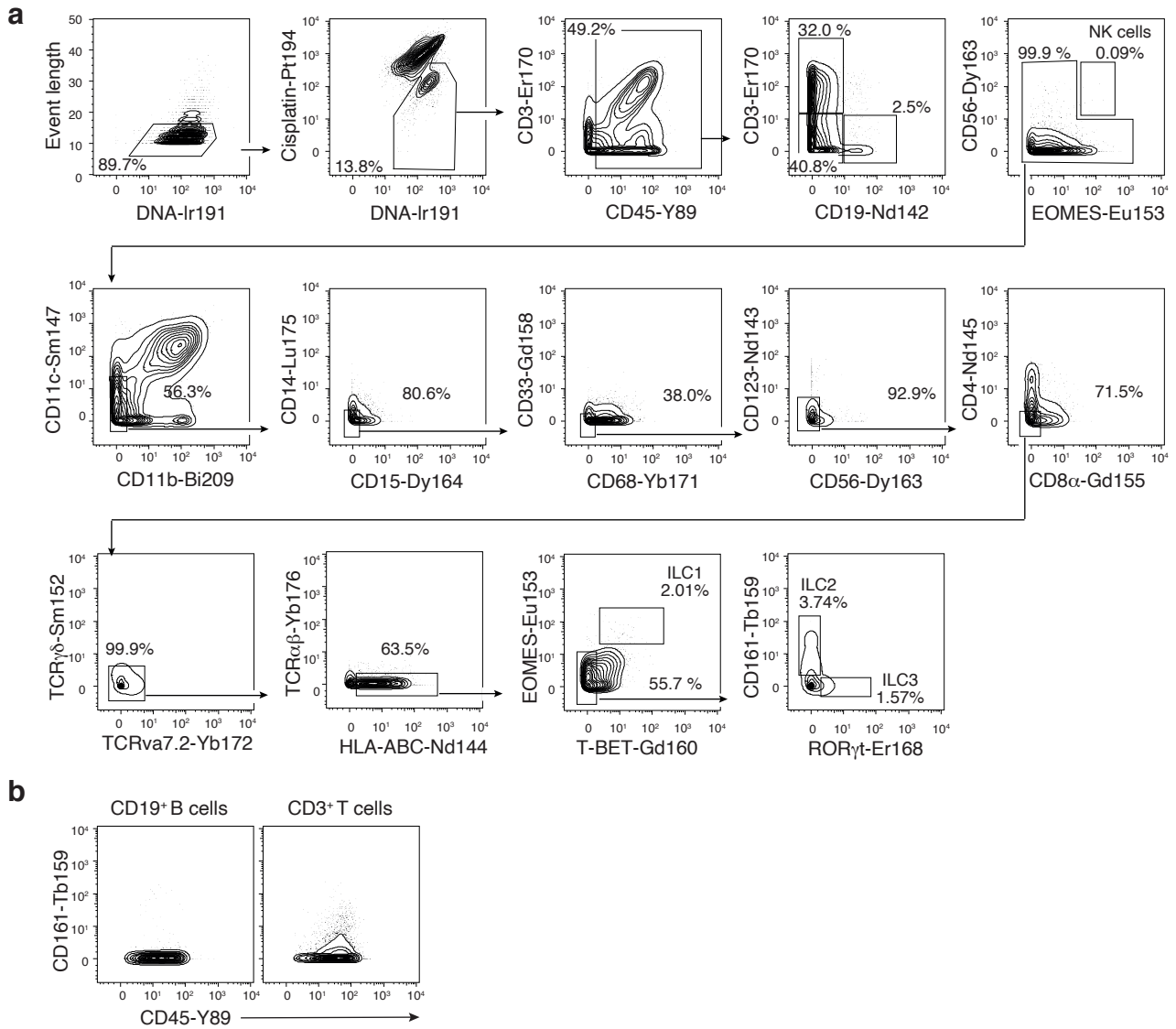
Group 1	Group 2	Mean difference (mm ²) and confidence intervals [Lower;Upper]	p value	Adjusted p value
<i>Rag1</i> ^{-/-}	C57BL/6J	23.052 [0.905;45.199]	0.0033	0.0479
<i>Rag2</i> ^{-/-} <i>Il2r</i> ^{-/-}	C57BL/6J	53.859 [25.995;81.723]	<0.0001	0.0007
<i>Rag2</i> ^{-/-} <i>Il2r</i> ^{-/-} +ILC2p	C57BL/6J	11.515 [-7.763;30.792]	0.0914	0.4639
<i>Rag2</i> ^{-/-} <i>Il2r</i> ^{-/-} +αLP	C57BL/6J	18.483 [-1.096;38.062]	0.0076	0.0458
<i>Rag2</i> ^{-/-} <i>Il2r</i> ^{-/-} +CLP	C57BL/6J	-8.052 [-28.262;12.158]	0.2602	1.0000
<i>Rag2</i> ^{-/-} <i>Il2r</i> ^{-/-}	<i>Rag1</i> ^{-/-}	30.807 [4.276;57.337]	0.0010	0.0403
<i>Rag2</i> ^{-/-} <i>Il2r</i> ^{-/-} +ILC2p	<i>Rag1</i> ^{-/-}	-11.538 [-28.831;5.756]	0.0594	1.0000
<i>Rag2</i> ^{-/-} <i>Il2r</i> ^{-/-} +αLP	<i>Rag1</i> ^{-/-}	-4.569 [-22.198;13.060]	0.4638	1.0000
<i>Rag2</i> ^{-/-} <i>Il2r</i> ^{-/-} +CLP	<i>Rag1</i> ^{-/-}	-31.104 [-49.431;-12.777]	<0.0001	0.0070
<i>Rag2</i> ^{-/-} <i>Il2r</i> ^{-/-} +ILC2p	<i>Rag2</i> ^{-/-} <i>Il2r</i> ^{-/-}	-42.344 [-66.531;-18.158]	<0.0001	0.0004
<i>Rag2</i> ^{-/-} <i>Il2r</i> ^{-/-} +αLP	<i>Rag2</i> ^{-/-} <i>Il2r</i> ^{-/-}	-35.376 [-59.804;-10.949]	<0.0001	0.0009
<i>Rag2</i> ^{-/-} <i>Il2r</i> ^{-/-} +CLP	<i>Rag2</i> ^{-/-} <i>Il2r</i> ^{-/-}	-61.911 [-86.847;-36.975]	<0.0001	0.0008
<i>Rag2</i> ^{-/-} <i>Il2r</i> ^{-/-} +αLP	<i>Rag2</i> ^{-/-} <i>Il2r</i> ^{-/-} +ILC2p	6.968 [-6.885;20.821]	0.1552	1.0000
<i>Rag2</i> ^{-/-} <i>Il2r</i> ^{-/-} +CLP	<i>Rag2</i> ^{-/-} <i>Il2r</i> ^{-/-} +ILC2p	-19.567 [-34.298;-4.835]	0.0002	0.0240
<i>Rag2</i> ^{-/-} <i>Il2r</i> ^{-/-} +CLP	<i>Rag2</i> ^{-/-} <i>Il2r</i> ^{-/-} +αLP	-26.535 [-41.659;-11.410]	<0.0001	0.0044

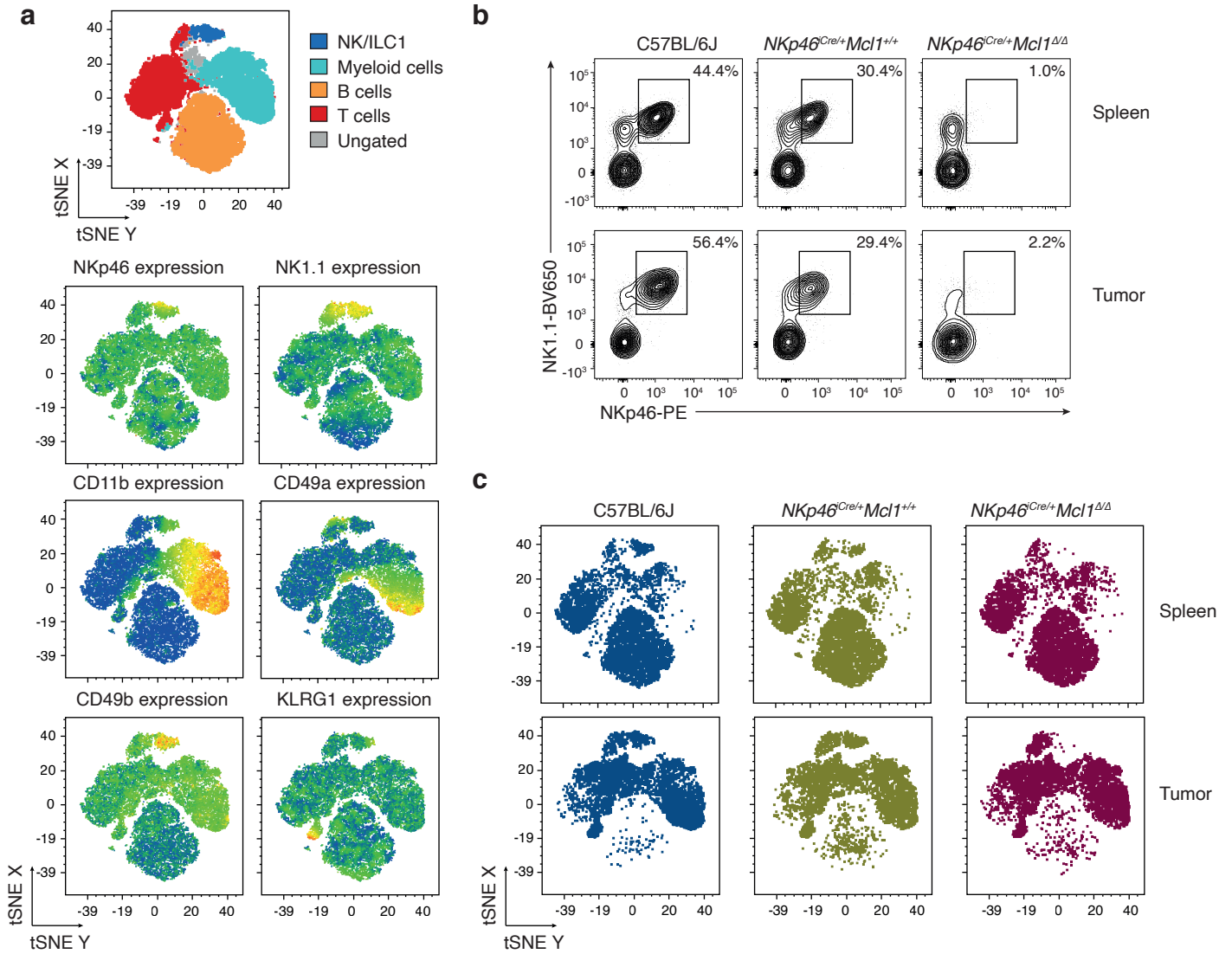
Note: Day 12-13 statistical analyses were performed using the tool web-based software TumGrowth with ANOVA followed with pairwise comparisons with Bonferroni adjustments.

Supplementary Table 3. List of genes used to derive the ILC2/Type 2 immune cell probability signature.

Feature	Gain	Cover	Frequency	Importance
<i>CD2</i>	0.67496245	0.21949935	0.08571429	0.67496245
<i>CCR7</i>	0.09781364	0.05139552	0.08571429	0.09781364
<i>GATA3</i>	0.05958073	0.05926664	0.12380952	0.05958073
<i>KLRG1</i>	0.0355216	0.1461106	0.07619048	0.0355216
<i>CD96</i>	0.02223839	0.00886725	0.04761905	0.02223839
<i>NFATC2</i>	0.01595909	0.01469443	0.03809524	0.01595909
<i>IL17RB</i>	0.01475181	0.03865042	0.04761905	0.01475181
<i>IL2RB</i>	0.01427828	0.01336656	0.02857143	0.01427828
<i>CD84</i>	0.01052721	0.00371385	0.01904762	0.01052721
<i>TNFSF10</i>	0.00737082	0.00296246	0.01904762	0.00737082
<i>IFITM2</i>	0.00730188	0.00297932	0.01904762	0.00730188
<i>CD53</i>	0.00602527	0.00383254	0.03809524	0.00602527
<i>MYD88</i>	0.00573675	0.08502729	0.04761905	0.00573675
<i>LCP1</i>	0.00323415	0.02896428	0.03809524	0.00323415
<i>EWSR1</i>	0.00283493	0.00086064	0.00952381	0.00283493
<i>PTGS2</i>	0.00242406	0.03578547	0.01904762	0.00242406
<i>TNFRSF9</i>	0.00234786	0.05041894	0.02857143	0.00234786
<i>CCR2</i>	0.00230522	0.03383285	0.01904762	0.00230522
<i>TXNIP</i>	0.00212972	0.03214757	0.02857143	0.00212972
<i>STAT4</i>	0.00209391	0.01679707	0.00952381	0.00209391
<i>JAK1</i>	0.00172269	0.00085682	0.00952381	0.00172269
<i>HLA-DMA</i>	0.00165005	0.00235477	0.01904762	0.00165005
<i>ILF3</i>	0.00161134	0.00083413	0.00952381	0.00161134
<i>ST6GAL1</i>	0.00159914	0.00434544	0.00952381	0.00159914
<i>CCR6</i>	0.00141219	0.02001168	0.01904762	0.00141219
<i>KLRB1</i>	0.00052743	0.00057376	0.00952381	0.00052743
<i>TNFAIP3</i>	0.00043063	0.0007577	0.00952381	0.00043063
<i>FAS</i>	0.00041605	0.03196678	0.01904762	0.00041605
<i>IFI35</i>	0.00032945	0.01663902	0.00952381	0.00032945
<i>CD37</i>	0.00029067	0.03207703	0.01904762	0.00029067
<i>TCF7</i>	0.00028846	0.01678255	0.00952381	0.00028846
<i>TRAF3</i>	0.00013665	0.01602485	0.00952381	0.00013665
<i>IRAK4</i>	9.51E-05	0.00374181	0.00952381	9.51E-05
<i>CTSS</i>	5.24E-05	0.00386062	0.00952381	5.24E-05







Unfractionated bone marrow cells

